Iraqi Journal of Science, 2026, Vol. 67, No. 2, pp: 599-612
DOI: 10.24996/ijs.2026.67.2.3

ISSN: 0067-2904

Removal of Rh 6G and DB 71 Dyes from Aqueous Solution with High Efficiency via Adsorption on Mesoporous Silica Nanoparticles

Zahraa Adel *, Ennas Abdul Hussein
Department of Chemistry, College of Science for Women, Baghdad, Iraq.

Received:30/6/2024 Accepted:6/2/2025 Published: 2026/2/28

Abstract

The use of mesoporous silica to remove cationic and ionic dyes from aqueous solutions has been investigated. This is a crucial process, as these dyes are widely recognized as a significant water pollutant, posing a threat to aquatic life, human health, and agricultural productivity. Cetyltrimethylammonium bromide (CTAB) served as a template and sodium silicate, a cost-effective silica precursor, was used in the Sol-gel process. The silica particles were characterized using N_2 adsorption–desorption isotherms, TEM, XRD, and SEM. The results indicate that mesoporous silica (MPS) particles in the nano range (40-80 nm) have the form of flower particles, with an average pore width of 3.44 nm, a precise surface area of 423.52 m^2g^{-1}, and a pore volume of 0.5677 cm^3/g. These particles may effectively adsorb dyes. The Langmuir, Freundlich, and Timken models of adsorption suited the adsorption equilibrium data, and the best-fitting isotherm model was determined using the linear regression coefficient R^2. A variety of thermodynamic parameters have also been assessed, including standard enthalpy change, entropy, and Gibb's free energy of the ongoing process of adsorption. The exothermic adsorption process was spontaneous, according to the thermodynamic data. The two dyes exhibited different kinetics: Direct Blue 71 (DB71) followed pseudo-first-order kinetics, while Rhodamine 6G (Rh6G) adhered to dye and pseudo second order rate kinetics. Kinetic data were obtained using a batch approach.

Keywords: Mesoporous Silica, Rh6G dye, DB71 dye, Adsorption, Isotherm.

إزالة صبغتي Rh 6G و DB 71 من المحلول المائي بكفاءة عالية عن طريق الامتزاز على جسيمات السيليكا النانوية المسامية

زهراء عادل ,ايناس عبد الحسين

قسم الكيمياء ,كلية العلوم للبنات, جامعة بغداد

الخلاصة

تم التحقيق في استخدام السيليكا المسامية لإزالة الأصباغ الكاتيونية والأيونية من المحاليل المائية. هذه عملية حاسمة، حيث تُعرف هذه الأصباغ على نطاق واسع بأنها ملوث كبير للمياه، وتشكل تهديدًا للحياة المائية وصحة الإنسان والإنتاجية الزراعية. عمل بروميد سيتيل ثلاثي ميثيل أمونيوم (CTAB) كقالب وتم استخدام سيليكات الصوديوم، وهو سلائف السيليكا الفعالة من حيث التكلفة، في عملية Sol-gel. تم توصيف جزيئات السيليكا باستخدام معادلات امتصاص-امتصاصN_2 ، والمجهر الإلكتروني النافذ، وXRD، والمجهر الإلكتروني الماسح. تشير النتائج إلى أن جزيئات السيليكا المسامية (MPS) في النطاق النانوي (40-80 نانومتر) لها شكل جزيئات زهرة، بعرض مسام متوسط يبلغ 3.44 نانومتر، ومساحة سطح دقيقة تبلغ 423.52 متر مربع $^{-1}$، وحجم مسام يبلغ 0.5677 سم مكعب / جم. قد تمتص هذه الجزيئات الأصباغ بفعالية. كانت نماذج الامتزاز Langmuirو Freundlich و Timken مناسبة لبيانات توازن الامتزاز، وتم تحديد نموذج تساوي درجة الحرارة الأفضل باستخدام معامل الانحدار الخطي R^2. كما تم تقييم مجموعة متنوعة من المعلمات الديناميكية

*Email: Zahraa.adel2305m@csw.uobaghdad.edu.iq

الحرارية، بما في ذلك التغير في المحتوى الحراري القياسي، والإنتروبيا، وطاقة جيب الحرة لعملية الامتزاز المستمرة. كانت عملية الامتزاز الطاردة للحرارة عفوية، وفقًا للبيانات الديناميكية الحرارية. أظهرت الصبغتان حركية مختلفة: اتبعت Direct Blue 71 (DB71) حركية شبه الدرجة الأولى، بينما التزمت Rhodamine 6G (Rh6G)بالصبغة وحركية معدل شبه الدرجة الثانية. تم الحصول على بيانات الحركية باستخدام نهج الدفعة.

Introduction:

The increasing use of various dyes is leading to significant environmental concerns regarding wastewater contamination [1, 2]. Many industries utilize wide-ranging of dyes to color their products, resulting in the release of substantial amounts of effluent into the environment, some of which are highly poisonous and could have a negative impact on the environment [3]. Consequently, dye contamination in water bodies has become a critical environmental issue. Wastewaters containing dyes are believed to be highly challenging for treatment because the dyes resist oxidizing agents and aerobic digestion [4, 6]. Dyes are being removed using a variety of chemical, physical, and biological treatment techniques [7, 10]. Physical-chemical adsorption is the least expensive and most straightforward of these techniques. Activated-carbon is widely regarded as an effective material for dye removal; investigations into the removal of dyes have focused on unconventional adsorbents such as wood [11], silica [12], clay and activated-clay [13], and residues of agricultural activities [14], due to their highly lower cost and the associated 10-15% regeneration loss. Large surface area and porosity mesoporous materials have been researched in great detail due to their wide range of applications in several fields, including adsorption, sensors, controlled-release delivery systems, and catalysis [15, 19]. The use of mesoporous silica nanoparticles (MSNPs) as a nano adsorbent to extract pigments from wastewater has been investigated [6, 20, 22]. The purpose of this study was to assess the adsorption capacity of mesoporous silica for the removal of Direct Blue71(DB71) and Rhodamine 6G (Rh6G) dyes from aqueous solutions using method [23, 25].

Materials and Methods:

In this study, sodium-silicate (14% NaOH, 27% SiO_2) was employed as a precursor for silica. CTAB, or cetyltrimethylammonium bromide was acquired from the State Company of Vegetable Oils - Iraq. Direct Blue71 (DB71) dyes, which has a molar mass of 1029.87 g/mol and a λ max at 578 nm, and rhodamine 6G, with a molar mass of 479.02 g/mol and a purity of 98% were sourced from DSM; their structures are displayed in Figure (1).

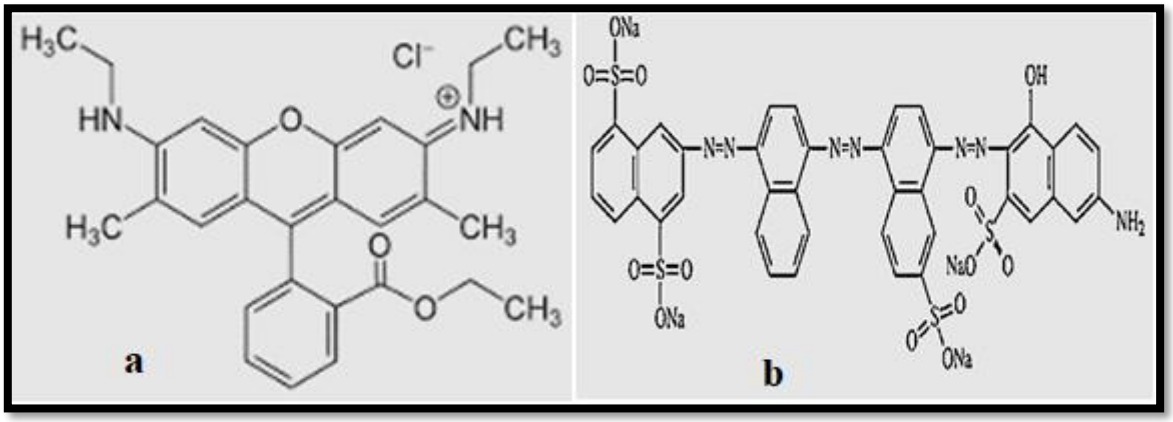

Figure 1: Chemical structure of (a) Rhodamine 6G (Rh6G) (b) Direct Blue71 (DB71).

Characterization:

The size and morphology of the produced nanostructures were evaluated using transmissioan electron microscopy (TEM, Philips model: CM120) and field emission high-resolution scanning electron microscopy (SEM; Oxford instruments model SEM: S-3200N). Using an Autosorb-1 Quanta chrome Instrument spectrometer (Quanta chrome Instruments, Boynton Beach, FL, USA), the N_2 adsorption–desorption isotherms at 77 K were recorded to determine the specific surface area of the samples. Via employing Cu Kα (λ = 0.154 nm) radiation. X-ray diffraction (XRD) patterns were generated using a Rigaku Diffractor-meter.

Preparation of Adsorbent :

Preparation of Mesoporous silica surface ($mSiO_2$)

In this study, a modified procedure was employed to prepare the sample [26]. Specifically, 0.9 g of CTAB was dissolved in 75mL of distilled water, and 75 mL of ethanol was added in a round bottom flask with stir. A total of 3.5g of sodium silicate dissolved in 150 ml of distilled water was added to the mixture drop by drop over the course of three hours using the burette. The surfactant was eliminated by calcinations at 600 °C for four hours after repeating for twenty-four hours, filtering, and drying at 80 °C for six hours.

Studies of Batch Mode Adsorption:

Batch-mode-adsorption studies were conducted for each dye to investigate the effects of various factors, including temperature, adsorbent dosage, and adsorbate concentration. A 250 ml capacity conical flask holding 50 mL of adsorbate at concentrations of (10 ppm Rh6G, 40 ppm DB71 was prepared, along with either 0.05 g or 0.06 g of adsorbent. The solution was shaken in a water bath shaker at 200 rpm on prearranged intervals. After fifteen minutes, the adsorbate solution was centrifuged at 3000 rpm. The concentration of the sample was measured using spectrophotometric determination. The following equation was used to calculate the amount of dyes adsorbed:

$$qe = (C_o - C_e)\, V/ W \text{ ----------(1)}$$

Where V (L) is the volume of dye solution, W (g) is the weight of the adsorbent, C_o and C_e are the concentration of the initial dye (mg L^{-1}) and at equilibrium, and qe is the equilibrium adsorption capacity of dyes adsorbed on unit mass of the adsorbent. The following calculation was used to calculate the percentage removal (R%) based on the dye concentration measurements:

$$R\% = (C_o - C_e) \times 100 / C_o \quad \text{---------- (2)}$$

Results and discussion:

Characterization of Adsorbent

Cu kα radiation (1.5406 Å) was used to obtain the XRD powder diffraction patterns using a for the small angle XRD diffractograms, respectively, were observed. The XRD pattern and small angle XRD of the $mSiO_2$ are presented Figures 2-a and 2-b. The low angle range of XRD patterns of the prepared mesoporous $mSiO_2$ exhibited well-resolved, strong diffraction peak at $2\theta = 4.19^o$ which characteristic a high intensity (100) peak indicating the formation of mesoporous structure. The small peak at $2\theta = 2.048$ characteristic to (110) and (200) peaks on the $mSiO_2$ indicating a high ordering of the pores. The board peak at 2θ 20-30 indicate that the mesoporous silica is amorphous. The crystalline size of $mSiO_2$ is (19.5) nm based on the data acquired and Scherer equation ($D = 0.92\ B \cos\theta$), where λ is the x-ray wave-length (Å), B is the FWHM (radian), and θ is the location (radian).

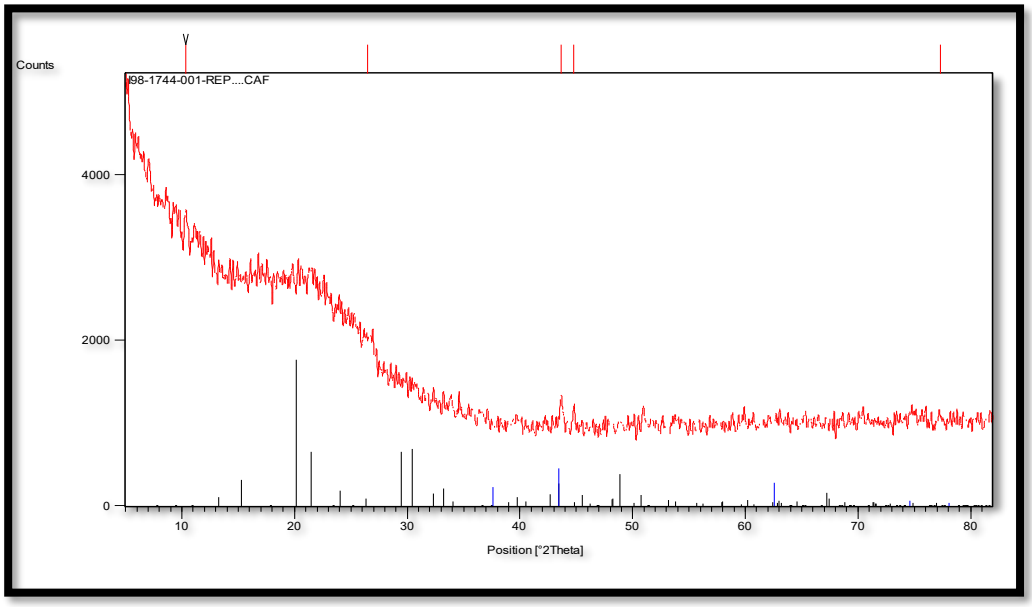

Figure 2-a: XRD patterns of sample $mSiO_2$.

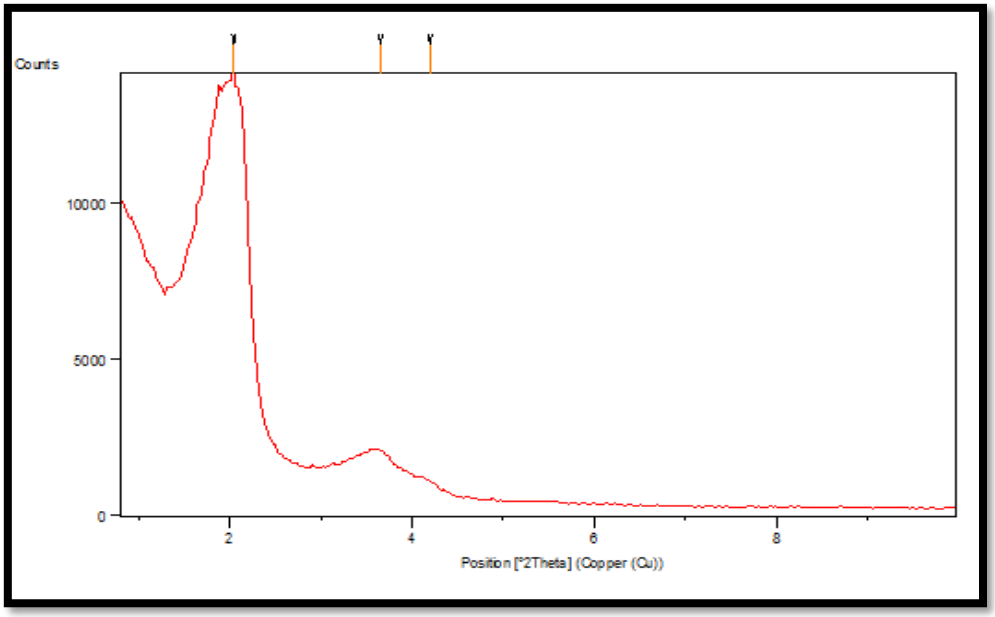

Figure 2-b: SMXRD patterns of sample $mSiO_2$.

Figure (3) presents SEM and EDX (Energy Dispersive X-Ray) micrographs of $mSiO_2$ nanoparticles, demonstrating the flower nanoscale structure of the particles with diameter range (20.03- 49.77) nm. Additionally, the TEM image of $mSiO_2$ shown in Figure (4) conferenced that the nanoscale particle sizes and the porous nature of $mSiO_2$.

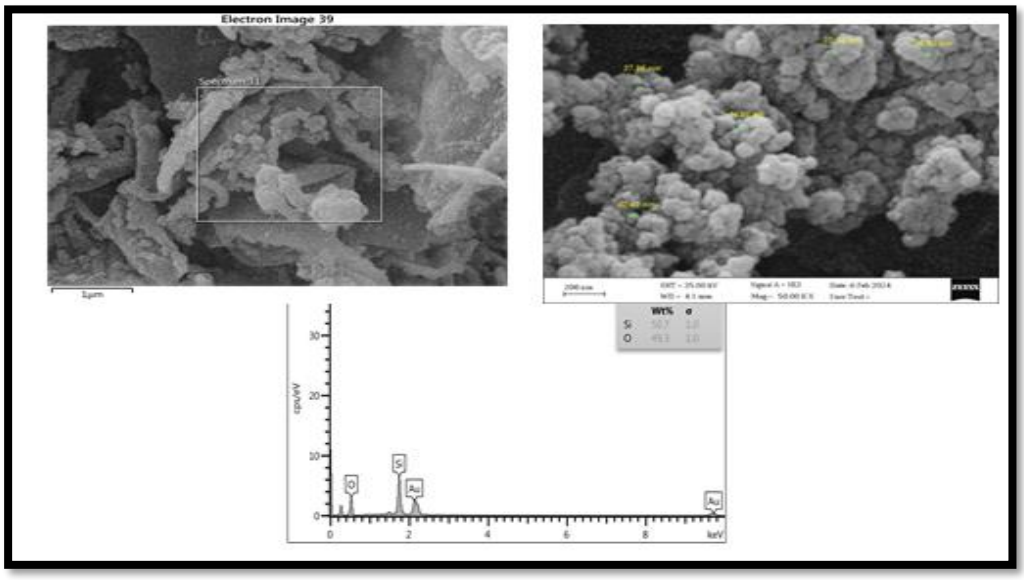

Figure 3: SEM and EDX Images for $mSiO_2$ sample.

Figure 4: TEM Image for $mSiO_2$ sample.

The N_2 adsorption-desorption isotherm and pore size distribution results demonstrate that mesoporous silica (MPS) particles in the nano range (40-80 nm), with an average pore width of 3.44 nm, a precise surface area of 423.52 m^2g-1, and a pore volume of 0.5677 cm^3/g, shown in Figure (5).

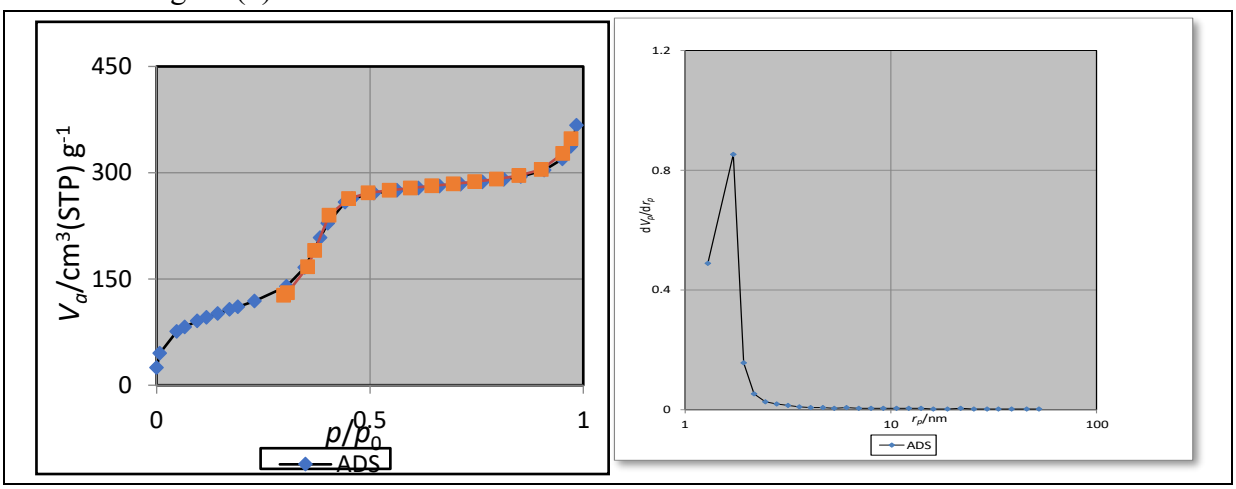

Figure 5: N_2 adsorption-desorption.

As is typical for mesoporous materials with structured pore architectures, the $mSiO_2$ isotherms displayed were classified as type IV b, indicating the presence of mesoporous similar to those found in ink bottles [27]. The desorption branch of the N_2 isotherm revealed that the average mesopore diameter (d BJH) of $mSiO_2$ was 3.44 nm.

Adsorption Study :

Effect of contact time and adsorbent quantity

Adsorption phenomena on the adsorbent and the diffusion of the adsorbate through the adsorbent are typically time-consuming processes. Figure (6) illustrates the effect of contact time on the adsorption of the two dyes onto $mSiO_2$. The impact of contact time and adsorbent quantity effects between dyes adsorbate and $mSiO_2$ adsorbent was studied in order to find solutions in which the concentration was (10) $mg.L^{-1}$ of Rh6G and (40) $mg.L^{-1}$ of DB71. Rh6G and DB71 exhibit fast adsorption at 10 minutes. Subsequently, a progressive increase in adsorption occurs with increasing contact time, reaching a maximum value of adsorption for Rh6G at 90 minutes and DB71 at 110 minutes. The adsorption capacity of DB71 grew gradually until it reached its maximum value at 110 (min.), at which point the curve plateaued. Consequently, the ideal contact time for DB71 is set at 110 (min), while for Rh6G, it is 90 min [28]. By varying the amount of adsorbent (0.01-0.06) g, per 100 ml in the test solution while maintaining the initial dye concentration (10ppm Rh6G, 40ppm DB71) and contact periods (90 minutes for Rh6G and 110 minutes for DB71) constant, the impact of adsorbent weight on the adsorption of the dyes was investigated. The increase in dye removal was minimal after doses of 0.05 g and 0.06 g, leading to their selection as the optimal adsorbent doses for further studies. Figure (6) presents the findings.

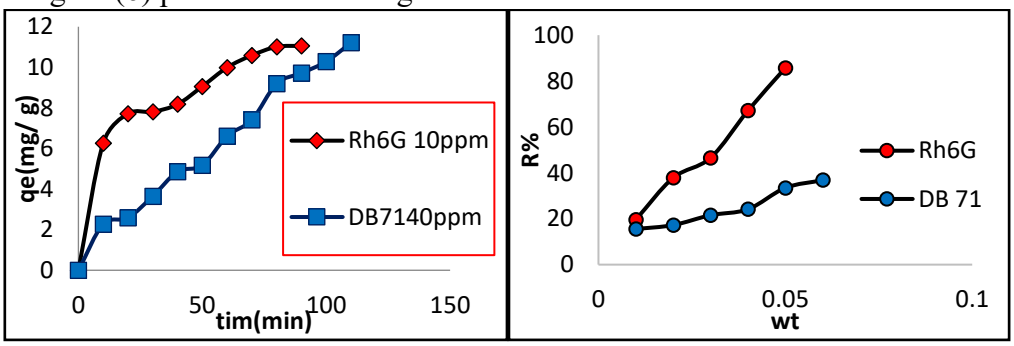

Figure 6: Contact time and Quantity effect of adsorbent on removing two dyes on $mSiO_2$.

Adsorption Isotherm by a mesoporous silica surface ($mSiO_2$)

Figure (7) presents the adsorption isotherms of the two dyes at 298K.The isotherms adsorption were of S-type According to Giles classification, which designating a vertical or flat orientation of adsorbate, additionally, the adsorbate is nonfunctional [29]. The adsorption process is reliant on the starting concentration, as demonstrated by Figure (7) which shows that the amount adsorbed of each dye increases with an increase in the original dye-concentration [30]. Results from temperature effect experiments indicate that the adsorption processes for both dyes are exothermic, as evidenced by an increase in the amount adsorbed when the temperature rises from 298 K to 323 K. In order to assess the effectiveness and costs of the adsorbent, adsorption data must be used to describe the behaviour of the adsorbent, adsorption isotherms, and the equilibrium distribution of solute between adsorbent and solution. Thus, this paper tested the three most often used isotherm equations: the Freundlich,

Temkin, and Langmuir models. The relevant values for the adsorption models of Langmuir (Eq.3), Freundlich (Eq.4), and Temkin (Eq.5) were determined by plotting the models using a conventional straight-line equation.

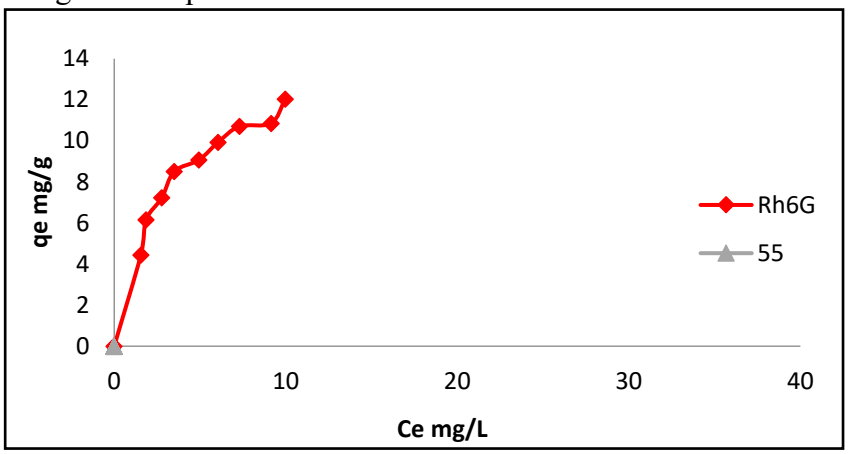

Figure 7: Adsorption isotherms of Rh6G and DB71 on $mSiO_2$ at 298K.

Adsorption isotherms:

1- lanmiur adsorption

$$qe = 1 / q_m \; K_L + Ce/ q_m \quad \text{----------(3)}$$

The quantity of dye adsorbed per gram of adsorbent is denoted by qe (mg/g), while Ce represents the equilibrium concentration of dye (mg/L). The maximum adsorption of n (mg/g) is denoted by q_m, and the Langmuir adsorption equilibrium is represented by K_L (L/mg), which are shown in Figures (8).

2- Frendulich adsorption

$$qe = K_f\,(Ce)\; 1/n \quad \text{----------(4)}$$

The Freundlich constants K_f and 1/n are associated with adsorption intensity and adsorption capacity, respectively, which are shown in Figures (9).

3- Temkin adslorption

$$qe = B \ln (K_t\, Ce) \quad \text{----------(5)}$$

The Temkin constants K_t (J/mol) and B (L/mg) are related to equilibrium binding and heat of adsorption, which are shown in Figures (10).

The two dyes Rh6G and DB71 yielded the linearized Langmuir, Freundlich, and Temkin isotherms, which are shown in Figures. together with the acquired parameters given in Table (1).

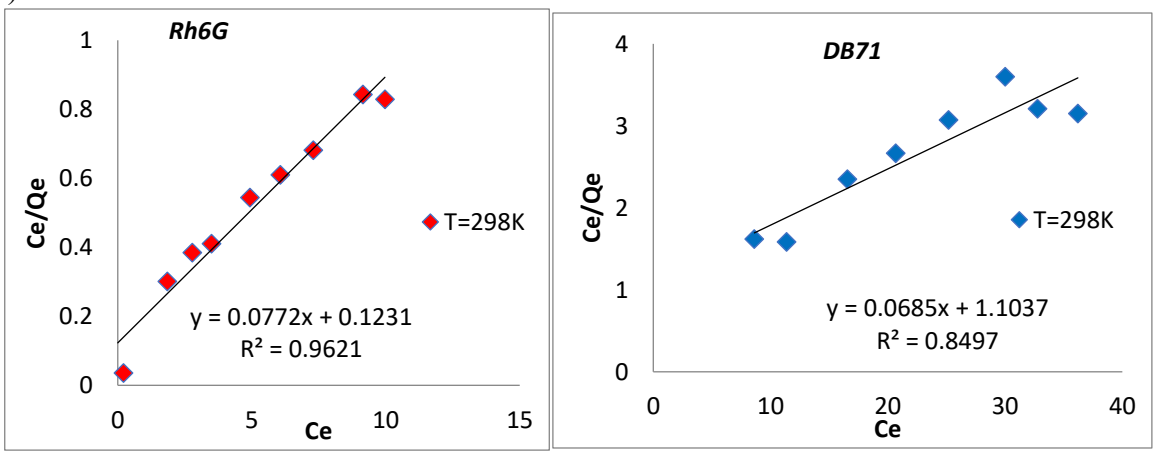

Figure 8: The liner plots of Langmuir equation for adsorption of Rh 6G and DB71 on $mSiO_2$ at 298K temperature.

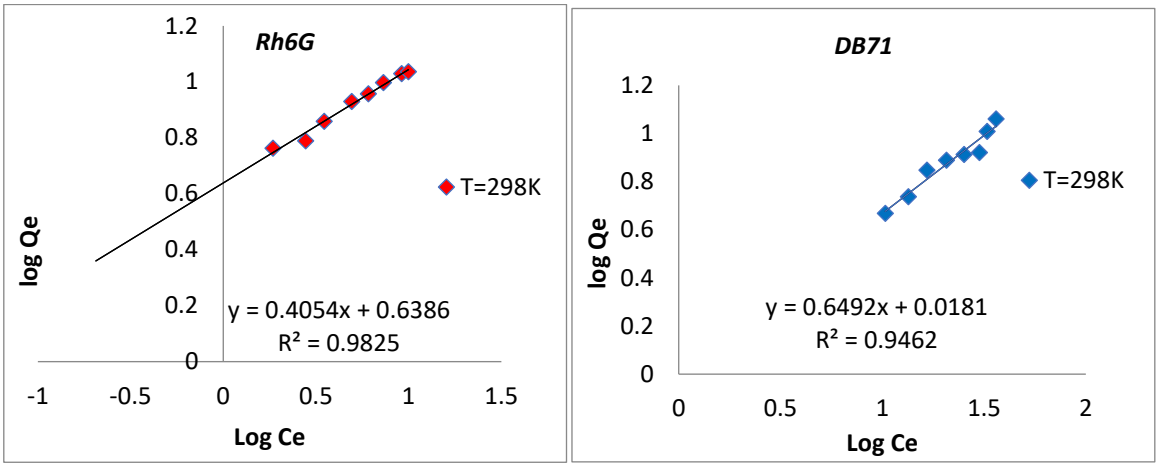

Figure 9: The liner plots of Freundlich equation for adsorption of Rh6G and DB71 on $mSiO_2$ at 298 K temperatures.

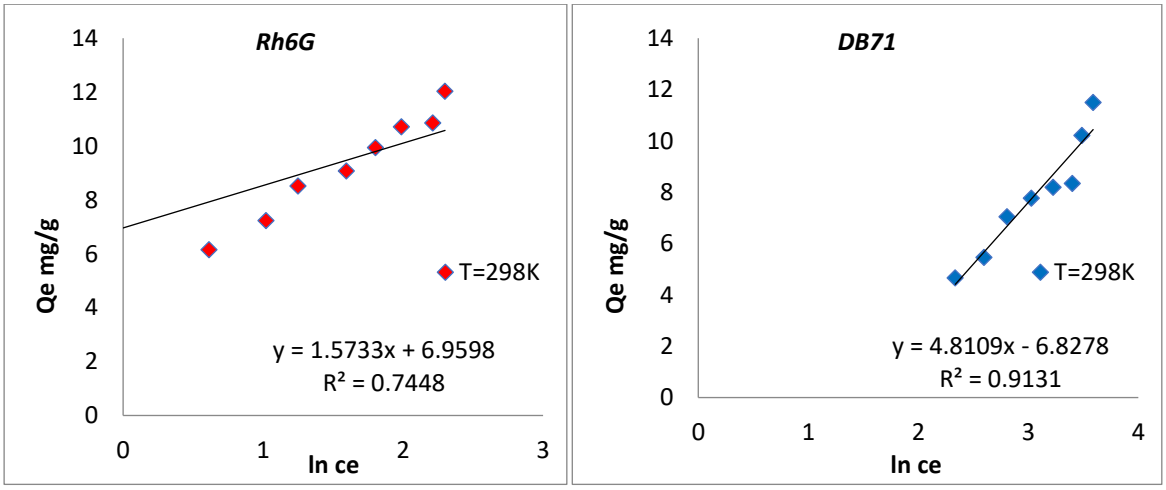

Figure 10: The liner plots of Temkin equation for adsorption of Rh6G and DB71 on $mSiO_2$ at 298K temperature.

Table 1: Langmuir, Freundlich and Temkin equation parameters for the two dyes on $mSiO_2$ adsorption at 298K temperature.

Dyes	Langmuir				Freundlich			Temkin		
	Q_m	K_L	R_L	R^2	1/n	K_f	R^2	B (L/mg)	K_t (J/mol)	R^2
Rh6G	12.95	0.627	7.3	0.962	0.61	3.09	0.982	1.57	83.4	0.74
DB71	14.59	0.062	3.5	0.849	0.65	1.05	0.946	4.81	0.25	0.913

The separation factor R_L is computed using the equation (6) to verify the adsorption process' favorability.

$$R_l = 1/\ 1+ K_l C_o \text{ ---------- (5)}$$

The R_L values indicate that the type of heat curve is irreversible $R_L = 0$), fit ($0 < R_L < 1$), linear $R_L = 1$) or not fit ($R_L > 1$), so the Langmuir is not fit, because the R_L values for the two dyes are ($R_L > 1$) [31], [32].

The comparison of R^2 values obtained from the Langmuir, Freundlich, and Temkin plots for two dyes indicates that the experimental data aligns best with the Freundlich isotherm, showing

R^2 values of 0.9825 for Rh6G and 0.9462 for DB71. The slopes of the isotherms, which were between 0 and 1, showed that the $mSiO_2$ nanoparticles were heterogeneous [33]. Additionally, large K_f values (1.05 for DB71 and 3.09 for Rh6G) showed that the nano-adsorbent exhibited a high affinity and high adsorption capacity.

Thermodynamics Analysis :

The equilibrium constant at different temperatures may be found using equation which says that $K_{eq} = qe / Ce$ [34, 32].

The equilibrium dye concentration in solution is represented by Ce, while the solid phase concentration at equilibrium is denoted by qe (mg/kg). Equations (6), (7) involving enthalpy change (ΔH^o), entropy change (ΔS^o), and free energy change (ΔG^o) were used to compute the corresponding values.

$$\Delta G^\circ = - RT \ln K \quad \text{---------- (6)}$$

$$\text{Ln } K_{eq} = - \Delta H^\circ / RT + \Delta S^\circ / R \quad \text{---------- (7)}$$

Values of ΔH° and ΔS° are measured Slope and intercept of the linear plots for ln K_{eq} vs 1/T, Figure (11).

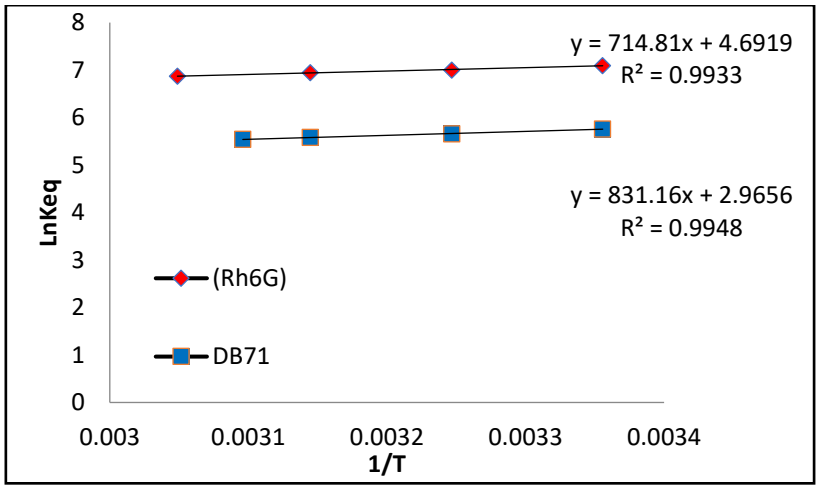

Figure 11: Van't Hoff plot of two dyes adsorption onto $mSiO_2$ for initial dye

Table 2 : Parameters of thermodynamic adsorption of the two dyes on $mSiO_2$.

Dyes	ΔH° KJ/mol	ΔS° J/K.mol	ΔG^o *KJ/mol*			
			298K	*308K*	*318K*	*328K*
Rh6G	-5.942	39.01	-17.58	-17.93	-18.36	-18.74
DB71	-6.91	24.656	-14.3	-14.5	-14.73	-15.11

The spontaneous nature of dye adsorption on porous silica is demonstrated by the negative values of ΔG^o for both dyes [25]. While a low negative value indicates low energy absorption at higher temperatures. The reaction is exothermic as the changes in enthalpy are negative at different temperatures [26]. The degree of freedom at the solid-liquid interface appears to increase after dye adsorption on porous silica, as evidenced by the positive values of ΔS^o for

RB6G and DB71. Based on entropy estimates, Rh6G and DB71 appear to have similar affinity for porous silica [27].

Kinetics Study:

The models of intraparticle diffusion kinetics, pseudo-second order, and pseudo-first order adsorption kinetics were investigated for the two dyes. The linearized form of Lagergren's pseudo-first order kinetic model is frequently employed [35].

$$\text{Log } (qe - qt) = \log qe - K_1 t \text{ ---------- (8)}$$

Where K_1 is the first-order adsorption rate constant and qt is the amount of dye adsorbed onto the adsorbent at time t.

In its integrated linear form, the pseudo-second-order kinetic mode is [36].

$$t / qt = 1 / qe_2 K_2 + 1 / qet \text{ ----------(9)}$$

Where K_2 is the second-order adsorption rate constant.

The Weber and Morris equation serves as the basis for the intra-particle diffusion kinetic model, which is [37].

$$qt = K_D t1/2 + C \text{ ----------(10)}$$

Whereas C is the intercept and K_D is the diffusion rate.

Table (3) contains the kinetic parameters that were determined by applying the three kinetic models to the experimental data. Figures 12, 13, and 14 display the linear plots of the three aforementioned equations.

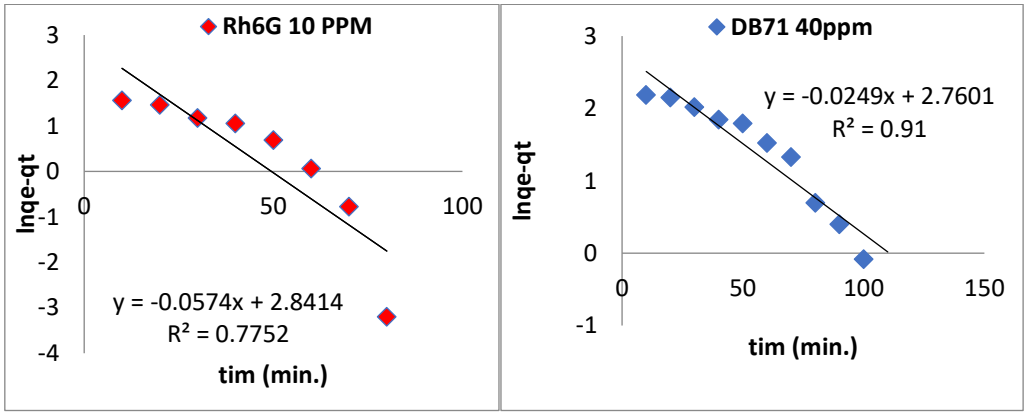

Figure 12: The pseudo-first order kinetic plot of the two dyes adsorption

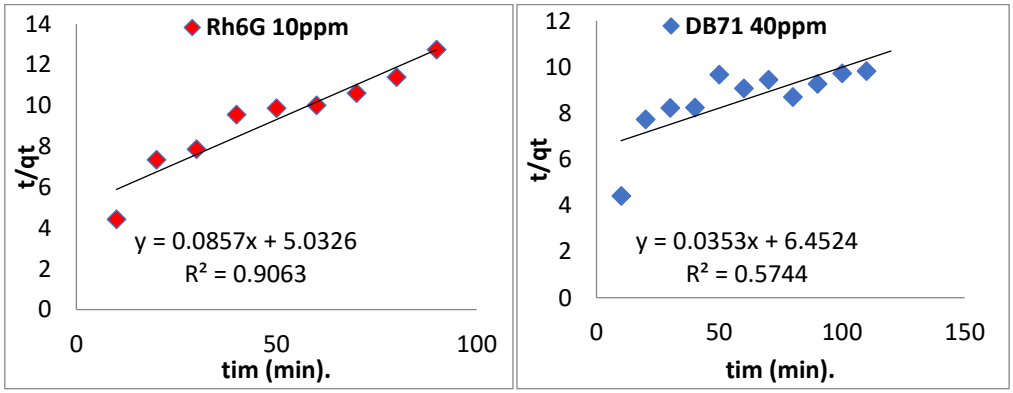

Figure 13: The pseudo-second order kinetic plot of the two dyes adsorption

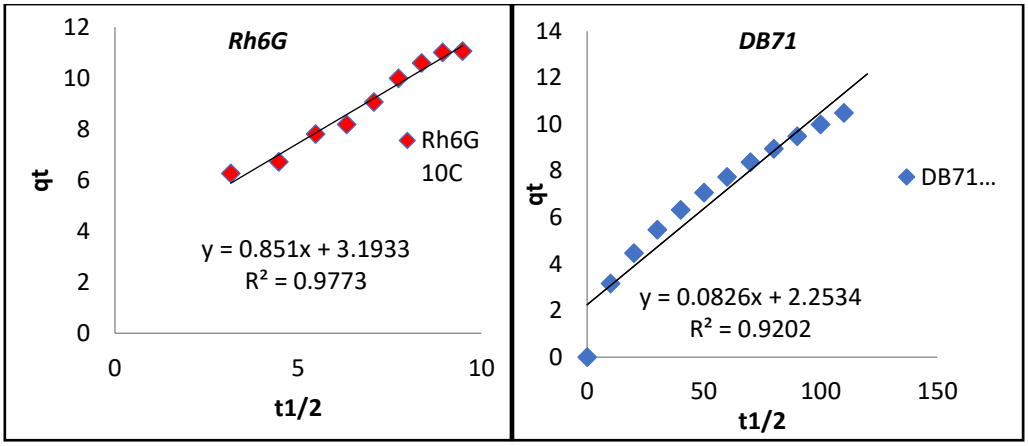

Figure 14: The intra-particle diffusion model of the two dyes adsorption on $mSiO_2$ at 298K.

Table 3 : Kinetic parameters for adsorption of Rh6G and DB71 on $mSiO_2$ at 298 K.

Rh6G								
qe (mg/g)	first -order			second –order				intrapartical diffusion
(exp.)	qe(calc) (mg/g)	K_1 (min^{-1})	R^2	qe(calc) (mg/g)	K_2 (g/mg. min)	h (mg $g^{-1}min^{-1}$)	R^2	K_2 (g/mg. min)
7.06	17.14	0.057	0.775	11.6686	1.4594×10-6	0.198	0.9063	0.851

DB71								
qe (mg/g)	first -order			second –order				intrapartical diffusion
(exp.)	qe(calc) (mg/g)	K_1 (min^{-1})	R^2	qe(calc) (mg/g)	K_2 (g/mg. min)	h (mg $g^{-1}min^{-1}$)	R^2	K_2 (g/mg. min)
11.206	15.801	0.0249	0.91	28.33	1.9312×10-7	0.145	0.5744	0.0826

The values of the correlation coefficient and (qe cale) for Rh6G and DB71 show that the first order model for DB71 and the second order model for Rh6G are determined to be more appropriate for explaining the adsorption kinetic data. The literature has also reported similar phenomena[38], [39]. Despite the linear regression of intraparticle diffusion, the figure did not pass through the origin, indicating that rate regulation involved steps other than adsorbent involving intraparticle [40]. The observation that the K2 values are lower than KD values suggests that the rate-limiting step in the process is intraparticle diffusion. The initial adsorption rate (h) was calculated from the intercept value of the plot of pseudo-second order model using the equation (11) [32, 41, 42].

$$h = K_2 . qe^2 \quad \text{----------} \quad (11)$$

Conclusion

Industrial wastewater often contains highly polluted, dyes, which negatively impact public water sources and can cause health problems. This type of pollution presents not only aesthetic problems, such as unpleasant odors and color changes, but also interferes with bathing and recreational activities, in addition to causing physical harm. Therefore, it is necessary to work on reducing these dyes and limiting the increase of wastewater pollution.

Our study approach includes finding an easy, inexpensive, and feasible method, which is the adsorption method of these dyes. The results of this study mentioned above confirm the fabrication of mesoporous silica nanoparticles as adsorption by the sol-gel method. The prepared sample exhibits a flower particle morphology, a specific surface area (423.52 $m^2 g^{-1}$), a pore volume (0.5677 cm^3/g), and an average pore diameter (5.362 nm). The results of the equilibrium adsorption were best described by the Freundlich equation. Thermodynamic analyses show that adsorption of Rh6G and DB71 dyes on mesopores was spontaneous, as well as exothermic on both.

Acknowledgements:

I am extremely grateful to Assistant Professor Dr. Ennas Abdul Hussein (Department of Chemistry/ Collage of Science for Women/University of Baghdad) for her technical support, extensive, assistance, and companionship in the field surveys which made the winter breeze and summer heat unforgettable.

References:

[1] A. Nishat, M. Yusufb, A. Qadir, Y. Ezaier, Viola Vambol, M. Ijaz, S. Moussa, H. Kamyab, S. Sehga, Ch. Prakash, H. Yang, H. Ibrahim, S Eldin, "Wastewater treatment: A short assessment on available techniques," *Alexandria Engineering Journal,* vol. 76, pp. 505–516. 2023, doi: 10.1016/j.aej.2023.06.054.

[2] T. A. Salman and M. I. Ali, "Potential Application of Natural and Modified OrangePeel as an Eco–friendly Adsorbent for Methylene Blue Dye," *Iraqi Journal of Science*, vol. 57, no. 1A, pp. 1–13, 2016.

[3] R. Al-Tohamy, S. Ali, K. Okasha, Y. Mahmoud, T.Elsamahy, H. Jiao, J. Sun, "A critical review on the treatment of dye-containing wastewater: Ecotoxicological and health concerns of textile dyes and possible remediation approaches for environmental safety," *Ecotoxicology and Environmental Safety*, vol. 231, p. 113160, 2022, doi: 10.1016/j.ecoenv.2021.113160.

[4] C. Valli Nachiyar, A. D. Rakshi, S. Sandhya, N. Britlin Deva Jebasta, and J. Nellore, "Developments in treatment technologies of dye-containing effluent: A review," *Case Studies in Chemical and Environmental Engineering,* vol. 7, p. 100339, 2023, doi: 10.1016/j.cscee.2023.100339.

[5] A. M. Hanna, K. M. Shareef, and L. O. Satar, "Kinetic Studies of Wastewater Purification Using Local Sand Samples in Erbil, Kurdistan," *Iraqi Journal of Science*, vol. 63, no. 7, pp. 2783–2792, 2022, doi: 10.24996/IJS.2022.63.7.3.

[6] H. Al- Rubai, A. Al-dahan, and B. Jasim, "View of Green Synthesis of Iron Oxide Nanoparticles and Their Modification with CTAB for the Decolorization of Dye Reactive Blue 238, " *Iraqi Journal of Science*, p1592-1600, 2023. doi.org/10.24996/ijs.2023.64.4.2

[7] M. Fauzi Abdullah, A. H. Jawad, N. F. Hanani Mamat, and K. Ismail, "Adsorption of methylene blue onto acid-treated mango peels: Kinetic, equilibrium and thermodynamic," *Desalination and Water Treatment*, vol. 59, pp. 210–219, 2016, doi: 10.5004/dwt.2016.0097.

[8] G. Bal and A. Thakur, "Distinct approaches of removal of dyes from wastewater: A review," *Materles Today Processes*, vol. 50, pp. 1575–1579, 2022, doi: 10.1016/j.matpr.2021.09.119.

[9] M. Y. Nassar, T. Y. Mohamed, I. S. Ahmed, and I. Samir, "MgO nanostructure via a sol-gel combustion synthesis method using different fuels: An efficient nano-adsorbent for the removal of some anionic textile dyes," *Journal of Molecular Liquids,* vol. 225, pp. 730–740, Jan. 2017, doi: 10.1016/j.molliq.2016.10.135.

[10] N. H. AL-Shammari and D. E. AL-Mammar, "Adsorption of Biebrich Scarlet Dye into Remains Chromium and Vegetable Tanned Leather as Adsorbents," *Iraqi Journal of Science*, vol. 63, no. 7, pp. 2814–2826, 2022, doi: 10.24996/IJS.2022.63.7.6.

[11] V. J. P. Poots, G. McKay, and J. J. Healy, "Removal of basic dye from effluent using wood as an adsorbent," *Water Pollution Control Federation, vol. 50, no. 5, pp*. 926–935, 1978,

Accessed: 2024.

[12] A. Ahmad, S. Jamil, Th. Choong, A. Abdullah,N. Faujan, A. Adeyi, R. Daik and N. Othman, "Removal of Cationic Dyes by Iron Modified Silica/Polyurethane Composite: Kinetic, Isotherm and Thermodynamic Analyses, and Regeneration via Advanced Oxidation Process," *Polymers (Basel).*, vol. 14, no. 24, p. 5416, 2022, doi: 10.3390/polym14245416.

[13] A. Espantaleón, "Use of activated clays in the removal of dyes and surfactants from tannery waste waters," *Applied Surface Science Advances journal*, vol. 24, no. 1–2, pp. 105–110, 2003, doi: 10.1016/S0169-1317(03)00153-4.

[14] S. Kainth, P. Sharma, and O. P. Pandey, "Green sorbents from agricultural wastes: A review of sustainable adsorption materials," *Applied Surface Science Advances journalAppl*, vol. 19, p. 100562, 2024, doi: 10.1016/j.apsadv.2023.100562.

[15] H. Zeng, X. Qu, D. Xu, and Y. Luo, "Porous Adsorption Materials for Carbon Dioxide Capture in Industrial Flue Gas," *Frontiers in Chemistry,* vol. 10, 2022, doi: 10.3389/fchem.2022.939701.

[16] Z. Duan, F. Cai, Y. Chen, T. Chen, and P. Lu, "Advanced Applications of Porous Materials in Triboelectric Nanogenerator Self-Powered Sensors," *Sensors*, vol. 24, no. 12, p. 3812, 2024, doi: 10.3390/s24123812.

[17] M. Farzan, R. Roth, J. Schoelkopf, J. Huwyler, V. Poots , G. McKay, and J. Healy, "Removal of basic dye from effluent using wood as an adsorbent," *Water Pollution Control Federation,* vol. 50, no. 5, pp. 926–935, 1978.

[18] P. Verma, Y. Kondo, Y. Kuwahara, T. Kamegawa, K. Mori, R.Raja "Design and application of photocatalysts using porous materials," *Catalysis Reviews,* vol. 63, no. 2, pp. 165–233, 2021, doi: 10.1080/01614940.2021.1948302.

[19] D. E. Al-Mammar and R. A. Mohammed, "Application of Surfactant for Enhancing the Adsorption of Azo Dye Onto Buckthorn Tree Wood Surface," *Iraqi Journal of Science*, pp. 1780–1798, Nov. 2017, doi: 10.24996/IJS.2017.58.4A.1.

[20] A. A. Mohammadi, A. A. Mohammad, A. Alinejad, B. Kamarehie, S. Javan, A. Ghaderpoury, M. Ahmadpour, M. Ghaderpoori "Metal-organic framework Uio-66 for adsorption of methylene blue dye from aqueous solutions," *International Journal of Environmental Science and Technology,* vol. 14, no. 9, pp. 1959–1968, 2017, doi: 10.1007/s13762-017-1289-z.

[21] S. M. Pourmortazavi, M. Rahimi-Nasrabadi, M. Aghazadeh, M. R. Ganjali, M. S. Karimi, and P. Norouzi, "Optimized routes for the preparation of gadolinium carbonate and oxide nano-particles and exploring their photocatalytic activity," *Desalin. Water Treat.*, vol. 74, pp. 316–325, 2017. doi: 10.5004/dwt.2017.20628.

[22] A. M. Alswieleh, "Efficient Removal of Dyes from Aqueous Solution by Adsorption on L-Arginine-Modified Mesoporous Silica Nanoparticles," *Processes*, vol. 10, no. 6, p. 1079, 2022, doi: 10.3390/pr10061079.

[23] P. O. Oladoye, M. Kadhom, I. Khan, K. H. Hama Aziz, and Y. A. Alli, "Advancements in adsorption and photodegradation technologies for Rhodamine B dye wastewater treatment: fundamentals, applications, and future directions," *Green Chemical Engineering*, vol. 5(4), pp. 440, 2023. doi: 10.1016/j.gce.2023.12.004.

[24] H. Li, V. L. Budarin, J. H. Clark, M. North, and X. Wu, "Rapid and efficient adsorption of methylene blue dye from aqueous solution by hierarchically porous, activated starbons®: Mechanism and porosity dependence.," *Journal of Hazardous Materials,* vol. 436, p. 129174, 2022, doi: 10.1016/j.jhazmat.2022.129174.

[25] D. AL-Mammar "V*iew of Adsorption of Brilliant Scarlet 3r dye onto Corn Silk as Agricultural Waste in Neutral Medium*," Iraqi Journal of Scienc, pp. 3606, 2024. doi.org/10.24996/ijs.2024.65.7.3

[26] E. Abdul-Hussein, S. Kareem,"*Studies on Mesoporous Silica preparation for Drug Delivery; Loading and Release Evaluation*," *Baghdad Science Journal,* , vol. 23, no. 5–8, pp. 361–362, 2021.

[27] A. A. Shiryaev, P. Pré, C. Pardanaud, V. Murzin, A. Averin, and J. N. Rouzaud, "Microporosity and nanostructure of activated carbons: characterization by X-ray diffraction and scattering, Raman spectroscopy and transmission electron microscopy," *Adsorption*, vol. 29, no. 5–6, pp.

275–289, 2023, doi: 10.1007/S10450-023-00406-X/METRICS.

[28] E. H. Mekatel, S. Amokrane, A. Aid, D. Nibou, and M. Trari, "Adsorption of methyl orange on nanoparticles of a synthetic zeolite NaA/CuO," *Comptes Rendus Chimie*, vol. 18, no. 3, pp. 336–344, 2015, doi: 10.1016/j.crci.2014.09.009.

[29] M. J. Iqbal and M. N. Ashiq, *"*Adsorption of dyes from aqueous solutions on activated charcoal,*" Journal of Hazardous Materials,* vol. 139, no. 1, pp. 57–66, 2007, doi: 10.1016/j.jhazmat.2006.06.007.

[30] M. Benjelloun, Y. Miyah, G. Akdemir Evrendilek, F. Zerrouq, and S. Lairini, "Recent Advances in Adsorption Kinetic Models: Their Application to Dye Types," *Arabian Journal of Chemistry*, vol. 14, no. 4, p. 103031, 2021, doi:10.1016/j.arabjc.2021.103031.

[31] J. Igwe and A. A. Abia, "Adsorption isotherm studies of Cd (II), Pb (II) and Zn (II) ions bioremediation from aqueous solution using unmodified and EDTA-modified maize cob," *Eclética Química*, vol. 32, no. 1, pp. 33–42, 2007, doi: 10.1590/S0100-46702007000100005.

[32] E. A. Dleam and S. H. Kareem, "Mesoporous Silica Nanoparticles as a System for Ciprofloxacin Drug Delivery; Kinetic of Adsorption and Releasing," *Baghdad Science Journa*l, vol. 18, no. 2, p. 0357, 2021, doi: 10.21123/bsj.2021.18.2.0357.

[33] M. Chen, C. R. Bowers, and W. Huang, "Silica-Encapsulated Intermetallic Nanoparticles for Highly Active and Selective Heterogeneous Catalysis," *Accounts of Materials Research Journal*, vol. 2, no. 12, pp. 1190–1202, 2021, doi: 10.1021/accountsmr.1c00153.

[34] J. Souad, N. Mahammed, "Kinetic and Thermodynamic Study of Methyl Orange Dye Adsorption on Zinc Carbonyldiphthalate, an Organometallic-Based Material Prepared with a Montmorillonite Clay," *Chemical Engineering Research and Design*, vol. 42, no. 1, p. 2023, 2023.

[35] R. Tseng, F. Wu, R. Juang , "Characteristics and applications of the Lagergren's first-order equation for adsorption kinetics," *Journal of the Taiwan Institute of Chemical Engineers*, vol. 41, no. 6, pp. 661–669, 2010, doi: 10.1016/j.jtice.2010.01.014.

[36] M. Benjelloun, Y. Miyah, G. Akdemir Evrendilek, F. Zerrouq, and S. Lairini, "Recent Advances in Adsorption Kinetic Models: Their Application to Dye Types," *Arabian Journal of Chemistry*, vol. 14, no. 4, p. 103031, 2021, doi: 10.1016/J.ARABJC.2021.103031.

[37] J. Wang and X. Guo, "Rethinking of the intraparticle diffusion adsorption kinetics model: Interpretation, solving methods and applications.," *Chemosphere*, vol. 309, no. Pt 2, p. 136732, 2022, doi: 10.1016/j.chemosphere.2022.136732.

[38] N. N gund, Marmatb, Salunkea, S. Jdokhes, A.Zine, S. Thore, S.Pardesh, "Removal of Rhodamine 6G from Aqueous Solution by Adsorption on Bio Adsorbent Prepared from Hyptis Suaveolens (Vilayti Tulsi): Kinetic, Equilibrium and Thermodynamic Study," *International Journal of Chemical Kinetics*, vol. 10, no. 3, pp. 1–9, 2021, doi: 10.30731/ijcps.10.3.2021.1-9.

[39] N. Mirzaei, A. H. Mahvi, and H. Hossini, "Equilibrium and kinetics studies of Direct blue 71 adsorption from aqueous solutions using modified zeolite," *Adsorption Science & Technology,* vol. 36, no. 1–2, pp. 80–94, 2018, doi: 10.1177/0263617416684836.

[40] L. M. S. Silva, M. J. Muñoz-Peña, J. R. Domínguez-Vargas, T. González, and E. M. Cuerda-Correa, "Kinetic and equilibrium adsorption parameters estimation based on a heterogeneous intraparticle diffusion model," *Surfaces and Interfaces*, vol. 22, p. 100791, 2021, doi: 10.1016/j.surfin.2020.100791.

[41] L. Gong, W. Sun, and L. Kong, "Adsorption of Methylene Blue by NaOH-modified Dead Leaves of Plane Trees," *Computational Water, Energy, and Environmental Engineering*, vol. 02, no. 02, pp. 13–19, 2013, doi: 10.4236/CWEEE.2013.22B003.

[42] Hu .Yuying, Pan Cheng , X.ohuan Zheng , Liu. Susu, Hu. Fengping , Li Xu and X. oming Peng , "Removal of ciprofloxacin with aluminum-pillared kaolin sodium alginate beads (CA-Al-KABs): Kinetics, isotherms, and BBD model," *Water (Switzerland)*, vol. 12, no. 3, 2020, doi: 10.3390/W12030905.